Pergamon

Journal of Structural Geology, Vol. 16, No. 8, pp. 1077 to 1092, 1994

0191-8141/94 $07.00+0.00

0191-8141(93)E0003-4

Multi-scale kinking in northeast Tasmania: crustal shortening at shallow crustal levels

BEN D. GOSCOMBE,* R. H. FINDLAY, M. P. MCCLENAGHAN and J. EVERARD

Tasmanian Department of Mines, P.O. Box 56, Rosny Park 7018, Tasmania, Australia

(*Received* 5 *January* 1993; *accepted in revised form* 20 *October* 1993)

Abstract—Analysis of S_1 cleavage trends in the Ordovician–Devonian Mathinna Group of northeast Tasmania has identified mega-scale (up to 9 km axial surface spacing) kink-bands and kink folds. These formed after the regional steep slaty cleavage and are contemporaneous with but post-date small-scale (cm-scale) vertical kink-bands. Small-scale sinistral kink-bands strike approximately 032° and predominate in number over the approximately E–W-striking dextral kink-bands. The geometry of the small-scale kink-bands indicates a 166° ± 10°-trending principal shortening during kinking. Kink-bands overprint minerals in the contact aureole of the Middle to Upper Devonian granite–granodiorite Scottsdale Batholith and pre-date deposition of the Parmeener Supergroup of Upper Carboniferous age. Megakinking in NE Tasmania is correlated with megakinking in the Lachlan Fold Belt (New South Wales) which occurred under the same bulk shortening direction and also during the Middle Carboniferous.

Prior to kinking, the regional slaty cleavage in the Mathinna Group was near vertical and trended 157°, which is subparallel to the principal shortening direction during kinking (166° ± 10°). Because of this close alignment and the presence of a pre-existing planar anisostropy throughout the region, megakinks developed despite only 4–5% bulk shortening. Kinking in NE Tasmania occurred at 120 ± 45 MPa (approximately 4.2 km depth). The brittle and 'instantaneous' nature of kinking is consistent with deformation at such shallow crustal levels. Megakinking may be a typical expression of crustal tectonics of minor bulk shortening at shallow crustal levels, only in the case of regions with a pre-existing steep planar structural grain subparallel to the principal shortening direction.

INTRODUCTION

NUMEROUS experimental and theoretical studies of kinking have been presented in the literature (Paterson & Weiss 1966, Gay & Weiss 1974, Weiss 1980, Williams & Price 1990, Stewart & Alvarez 1991). These are primarily concerned with the relationship between kink geometry and the principal shortening direction, and with the propagation of kink-bands. Some studies of natural kinks test experimental and theoretical models (Anderson 1964, Powell *et al.* 1985, Kimura *et al.* 1989, Stubley 1990, Stewart & Alvarez 1991), but few studies relate kinking and the scale of kinking to wider tectonic considerations such as the relationship of the principal shortening axis with respect to the pre-existing regional planar anisostropy, regional bulk shortening and depth of crustal residence.

Though small- to medium-scale (1 cm–50 m) kinking is a common upper-crustal late-stage feature of orogens, mega-scale (100 m–10 km) steeply plunging kinking is apparently rare, being previously reported only from the Ordovician–Devonian Lachlan Fold Belt in eastern Australia (Rixon *et al.* 1983, Powell *et al.* 1985, Stubley 1990). (Nevertheless, large-scale monoclines with shallow to horizontal axes are a common feature of fold–thrust belts world wide.) Although studies of kinking in the Lachlan Fold Belt constrain the bulk regional shortening and strain field they do not define the depth of crustal residence during kinking accurately. Such information is critical in confidently constraining models of crustal tectonics during megakinking. This study defines the depth at which kinking occurred in NE Tasmania, and outlines the geometry of all scales of kinking and the controlling strain field. Kink-band geometry and the kinematic analysis presented are based on detailed mapping and data collected from the central region of NE Tasmania (Fig. 1). The study was expanded to encompass the whole of the Mathinna Group in NE Tasmania through study of data contained in published Tasmanian Department of Mines 1:50,000 and 1:63,360 map sheets and accompanying reports; these give complete cover of the region.

REGIONAL GEOLOGY

The oldest rocks in NE Tasmania are the Lower Ordovician to Lower Devonian Mathinna Group (Baillie *et al.* 1989, Powell & Baillie 1992) (Fig. 1), a turbiditic sequence of alternating quartzwacke sandstones and siltstones–mudstones that comprise all the folded sedimentary sequences older than the unconformably overlying late Lower Devonian (388 ± 1 Ma) St Marys Porphyrite (Turner *et al.* 1986). The first deformation of the Mathinna Group (D_1) gave rise to tight chevron folding (F_1) on m- to km-scale around shallow to intermediate NNW- and SSE-plunging axes. Typical interlimb angles of 50–90° indicate maximum ENE–WSW crustal shortening during D_1 in the order of 30–55%. F_1 folding is pervasive in the Mathinna Group throughout all of NE Tasmania, producing a variably strong axial planar penetrative cleavage (S_1) that is the predominant structural surface throughout the whole region. For most of this region S_1 is very steep (more than 70°), but

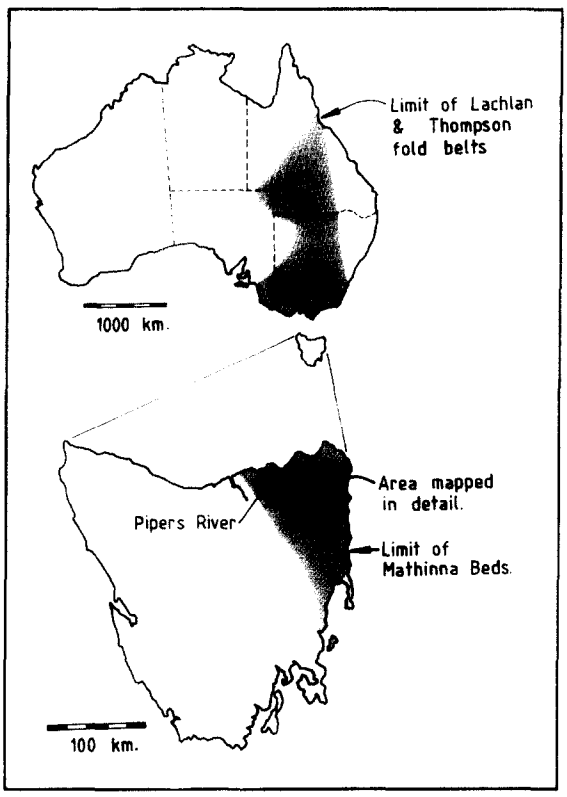

Fig. 1. Location of the area mapped in detail within NE Tasmania. Approximate limit of Thompson and Lachlan Fold Belts are after Powell *et al.* (1985).

S_1 dips gently westward in the Pipers River area (Marshall *et al.* 1969).

Granodiorite batholiths were emplaced coeval with the St Marys Porphyrite in the Middle Devonian and younger Adamellites and Alkali granitoids were emplaced during the Upper Devonian (Powell & Baillie 1992). Radiometric ages for all NE Tasmanian granitoids span 356–392 Ma (Cocker 1982). The second deformational event in NE Tasmania (D_2) involved WSW-directed thrusting of the whole region, crenulation cleavage development and reorientation of F_1 folds to recumbent orientations due to upramping of the Pipers River region (Powell & Baillie 1992). D_2 postdates the St Marys Porphyrite, deforms Middle Devonian granodiorites but not Middle to Upper Devonian adamellites, and is thought to be of Middle Devonian age (Powell & Baillie 1992).

Kink-bands (F_3) on all scales from mm- to km-scale were developed in the Mathinna Group throughout NE Tasmania. Kilometre-scale megakinking of Mathinna Group has resulted in sharply defined domains of constant S_1 strike that have been rotated 11–31° from the average S_1 strike (157°) in non-rotated domains throughout NE Tasmania. The non-rotated domains (strike 150–167°) have been termed SSE–NNW domains throughout this paper. The megakink domains (i.e. rotated domains) have been grouped according to their average S_1 strike as; SE–NW (140–150°), E–W (113–128°) and N–S (170–185°) domains.

Within the contact aureole of the Scottsdale Batholith small-scale kink-bands kink and fracture biotite and muscovite grains and fold flattened cordierite porphyroblasts into gentle arcs. Consequently, D_3 kinking postdates the granodiorite intrusion and therefore the maximum age of D_3 kinking is Upper Devonian and possibly younger than 356 Ma if the kinks post-date the younger adamellites as well (Cocker 1982). The only constraint on the minimum age is that the kinks pre-date the oldest sediments of the Parmeener Supergroup (approximately 300 Ma) because these sediments are flat lying and show no evidence of NNW–SSE shortening. An identical minimum age is offered for kinking of the Lachlan Fold Belt (Powell *et al.* 1985) which forms the basement of the post-300 Ma Sydney Basin. The maximum age limit of megakinks in the Lachlan Fold Belt is younger than 340–350 Ma and the kinks are thought to be of approximately 330 Ma age (Powell *et al.* 1985). Powell *et al.* (1985) correlates Middle Carboniferous kinking in eastern Australia with the N–S-directed compression associated with the Alice Springs Orogeny in central Australia.

METAMORPHIC GEOLOGY

Geothermobarometry has been used to constrain the depth of burial of the Mathinna Group at the time of Middle to Upper Devonian batholithic emplacement. The depth of crustal residence of the presently exposed rocks during D_3 kinking is interpreted to be equivalent to that during the time of granitoid intrusion. D_2 WSW-directed over-thrusting is reported to have deformed Middle Devonian granodiorites (Powell & Baillie 1992), thus the region could have potentially been thrust to shallower crustal levels prior to D_3 kinking. However, in central NE Tasmania (Fig.5) the D_2 event has not appreciably reoriented S_1 from its original subvertical orientation (Powell & Baillie 1992). Therefore, upramping in the study area is considered negligible.

The Upper Devonian granitoids contact metamorphosed the Mathinna Group, giving rise to 1–2 km wide aureoles of spotted metapelites. Typical assemblages in the metapelites are cordierite–muscovite–biotite–quartz–K-feldspar–ilmenite–rutile ± plagioclase ± andalusite. Such assemblages form at 400–600°C and less than 250 MPa as shown by comparison to experimental and theoretical phase stability data (Fig. 2).

The Hollister *et al.* (1987) calibration of the aluminium-in-hornblende geobarometer has been applied to seven granodiorite samples from the Scottsdale Batholith resulting in pressures of 15–200 MPa and averaging 90 MPa. These pressures are considered reliable because the whole-rock composition of the Scottsdale Batholith samples are equivalent to those used for the empirical calibration of this geobarometer. These low pressures are supported by results between 22 and 162 MPa and averaging 78 MPa derived from the experimentally calibrated hornblende geobarometer of Johnson & Rutherford (1989).

Our geobarometric calculations based on phengite (Massone & Schreyer 1987) and K-feldspar–biotite–muscovite (Bucher-Nurminen 1987) geobarometry of

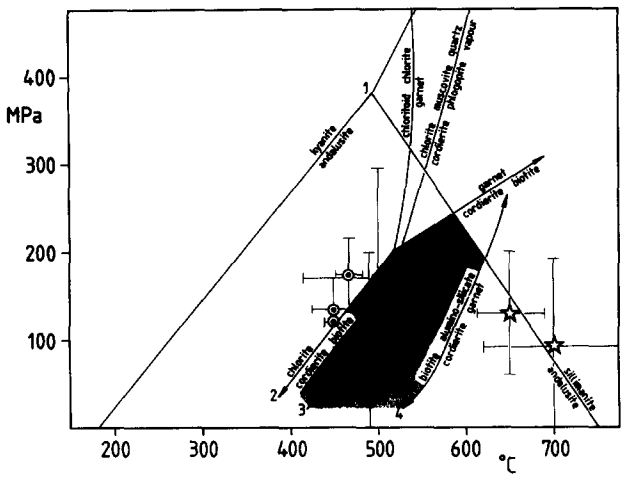

Fig. 2. Experimental and theoretically calculated phase equilibria for pelitic systems. Shaded region is the stability field of metapelite assemblages adjacent to the Scottsdale Batholith. Small dots in circles are the preferred *P–T* loci of metapelite samples. Bars indicate range of geothermobarometry results, not analytical errors. Solid dots are temperature estimates (with error bar), from metapelites based on equilibrium thermodynamics and assuming a pressure of 120 MPa. Dashed line is the average pressure result for one metapelite sample by equilibrium thermodynamics. Stars are preferred *P–T* loci of Scottsdale Batholith samples. Full analytical results are available in Goscombe *et al.* (1992). (1) Al-silicate triple point (Spear & Cheney 1989); (2) theoretically calculated equilibria in KFASH (Powell & Holland 1990); (3) experimentally derived equilibria in KMASH (Massone 1989); and (4) theoretically calculated equilibria in KFMASH (Spear & Cheney 1989).

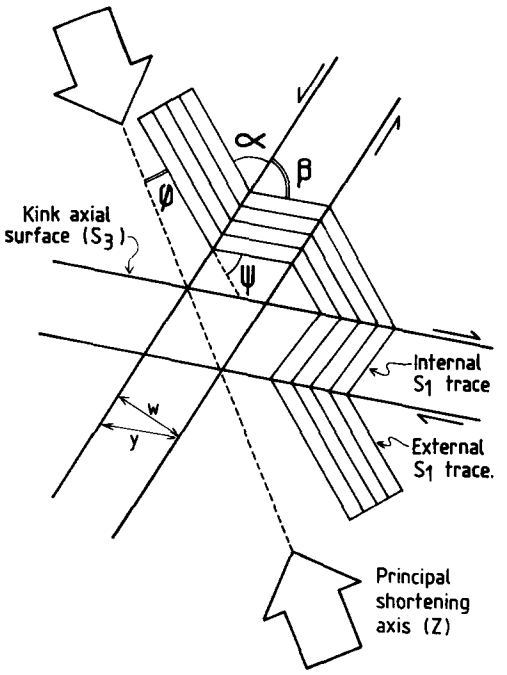

Fig. 3. Geometry of idealized conjugate 'reverse' kink-bands and definition of nomenclature and symbols. w = orthogonal width of kink-band, y = length of internal S_1 cleavage trace within kink-band. Further explanation in text.

five contact aureole metapelites require constraint by accurate and independent estimation of the temperature of equilibration. Temperatures of contact metamorphism were calculated using the biotite–muscovite geothermometer of Hoisch (1989) for all samples, and additionally plagioclase–K-feldspar (Powell & Powell 1977) and biotite–chlorite (Laird 1989) geothermometry in two samples. Temperatures of formation range 450–500°C and constrain the geobarometry results to a range of 100–175 MPa (Fig. 2).

Average pressure and average temperature calculations were performed on three metapelite samples using the equilibrium thermodynamics method of Powell & Holland (1988). All calculations were carried out using the program THERMOCALC v1.2 (R. Powell personal communication 1990). For temperatures of 500–550°C the average pressure is 30–160 MPa. The calculated average temperatures of 534–544°C, for a pressure estimate of 120 MPa, are slightly higher than temperature estimates by the geothermometry methods employed above (Fig. 2). Temperature estimates calculated by equilibrium thermodynamics may be more reliable as they are more consistent with the phase stability field of the metapelite assemblages (Fig. 2).

Pressure estimates by the four methods employed here are mutually consistent and together give a reliable estimate of the pressures during batholith emplacement. All pressure estimates are low (less than 200 MPa) and average around 120 ± 45 MPa (4.2 km depth). Such shallow levels of emplacement of NE Tasmanian batholiths is supported by the closely associated St Marys Porphyrite (Turner *et al.* 1986) and the very narrow contact aureoles (Goscombe *et al.* 1992).

SMALL-SCALE KINK-BANDS

General features

All kinking in outcrop possesses monoclinic 'reverse' (Dewey 1965) kink-band geometry. Kink-bands are planar with subparallel axial surfaces. They kink well-aligned phyllosilicates that define S_1 and within the kink-band this cleavage is active as slip surfaces to accommodate kinking. The kink-bands are best developed in shales and siltstones and only very rarely developed in silty sandstones. There is no alignment of mineral phases with the fold axial surfaces of the kink-bands, and no new mineral growth is seen to be associated with kinking. The axial surfaces are parallel for lengths typically greater than the width of the outcrop (exceeding 1–10 m). The kink-bands terminate by the low-angle convergence of the axial surfaces, forming a very elongate lenticular morphology. Small-scale kink-bands are also terminated by short (less than 2 cm long) microfaults with offsets smaller than 2 mm. These faults are parallel to and are continuations of the axial surface. Both the kink-bands and microfaults have the same shear sense.

Most kink hinges are angular and sharp in outcrop. In thin section the axial surface (S_3, Fig. 3) is planar to curviplanar and also rarely bifurcates. The kink hinge zone is most commonly a single axial surface but may also comprise an en échelon set of discontinuous axial surfaces inclined at low angles. In thin section some of

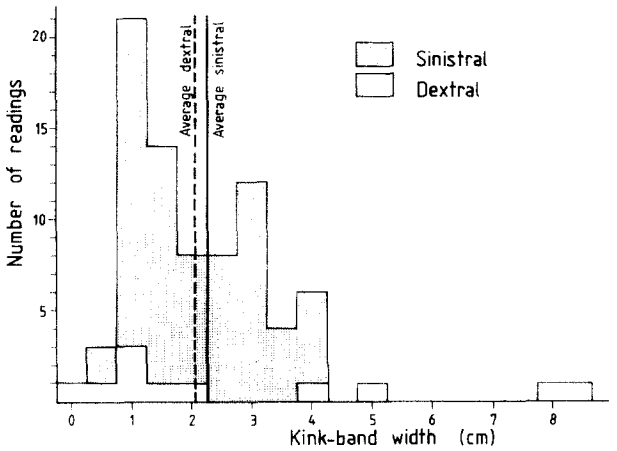

Fig. 4. Histogram summarizing all data on kink-band widths from the region mapped in detail. Only kink-bands with widths below 8 cm are included.

the kink hinges are not perfectly angular but slightly rounded and typically form a hinge zone of up to 0.4 mm wide. More rounded hinges comprising a wider hinge zone (up to 3 mm) have been observed in outcrop.

Orthogonal to the axial surface both sinistral and dextral kink-bands range in width (Fig. 3) from 1 to 200 mm with very few over 40 mm. The average sinistral kink-band width is 23 mm and the average dextral kink-band is 21 mm wide (Fig. 4). Kink-bands have been traced for up to 10 m in length, the limit of the exposure, and may be considerably longer. These dimensions are of the same order as those described by Lennox (1980) from the region immediately south of our study area. Second-order kink-bands, 1–10 m wide, are known to occur from changes in the orientation of S_1 between successive outcrops. These kinks cannot be mapped because of the lack of continuity between outcrops. This scale of kinking is not common and only recognized in domain C (Fig. 5), and not treated further in this study.

The number of small-scale kink-bands per metre along sections parallel to the local S_1 strike has been recorded from 23 localities. The range is 0.33–4.00 kink-bands m^{-1} and the average is 2.11 kink-bands m^{-1}. Some outcrops have no kink-bands (especially in domain A), and these values therefore only give an indication of the maximum spatial density of kink-bands for the region mapped in detail.

Sinistral kink-bands are tightly constrained in strike throughout the region mapped in detail, averaging 032°. All kink-bands dip steeply (70–90°) and display no asymmetry in the direction of dip (Fig. 6). The average sinistral S_3 strike in each domain ranges between 031° and 045° (Fig. 7). The dextral kink-bands are subvertical (85–90°) but have a significant range in strike throughout the area (48–127°). The average dextral S_3 strike is 89° (Fig. 6). The strike of dextral kink-bands in domain C is ENE, whereas in the SSE–NNW-domains (A and D) they strike ESE. Similarly sinistral kink-bands in domain C strike anticlockwise of those in the SSE–NNW-domains (Fig. 7). This suggests that both sinistral and dextral small-scale kink-bands were rotated in association with the bulk rotation of domain C as a result of megakinking (Fig. 5). Consequently, the small-scale kink-bands may have formed earlier than the megakinks.

The proportion of sinistral to dextral kink-bands (sin./sin.+dext.) varies between structural domains. For example only sinistral kink-bands are found in the E–W domain B (Fig. 5). SE–NW domain C has the next highest proportion of sinistral kink-bands (92%) and the average of all SSE–NNW domains (A, D, E, F and G) has the lowest proportion of sinistral kink-bands (64%) (Appendix 1). Thus the domains that have experienced greatest sinistral rotation due to megakinking have a greater dominance of sinistral kink-bands relative to dextral kink-bands.

Conjugate pairs of kink-bands are only rarely seen in outcrop. This is either because outcrops are typically small (less than 0.25 m^2) or conjugate pairs are rare. Conjugate kink-bands are reported by Threader (1967) and Lennox (1980) from within the area mapped in detail and further to the south. Thus, the steep sinistral and dextral kink-bands of NE Tasmania are considered to have formed together as conjugates.

The orientation of the kink axial surface with respect to the S_1 foliation outside the kinked domain is defined by the acute angle α (Fig. 3). Average α from each structural domain ranges from 65° to 78° in sinistral kink-bands and 50–83° in dextral kink-bands (Fig. 8 and Appendix 1). α-values increase progressively from within SSE–NNW to SE–NW and to E–W domains (Fig. 8 and Appendix 1). The orientation of the internal S_1 foliation with respect to the kink axial surface is the angle β (Fig. 3). β is always adjacent to the angle α, and β can potentially have values exceeding 90° typically in the case of 'normal' kink-bands ($\alpha + \beta > 180°$). Small-scale 'normal' kink-bands are, however, absent in the region studied. Average β angles from sinistral kink-bands of different structural domains range 58–73° (Fig. 8 and Appendix 1). The angle of rotation of the internal S_1 cleavage as a result of kinking is defined by the angle ψ (Fig. 3). The angle ψ is very tightly constrained to 36–45° for both sinistral and dextral kink-bands from all domains (Appendix 1). Measurements of α and β angles from small-scale kink-bands plot as a wide scatter either side of the constant volume ($\alpha = \beta$) line (Fig. 9). Most of the spread in this data is towards $\alpha > \beta$. This scatter indicates that the kink-bands have experienced volume loss, possibly by progressive shortening across the kink-band.

On a microscopic-scale, there are two distinct geometries of quartz-veinlets associated with the small-scale kinking.

(1) En échelon sets of short discontinuous lenticular veinlets form within and at consistently inclined low angles to the kink axial surface. These have ragged edges indicating ripping apart of phyllosilicates and dilation along an axis at a low angle to the S_1 cleavage. Such veinlets are thought to be due to brittle fracture and dilation in the hinge of the kink.

(2) Less commonly, long (up to 5 mm) but very thin planar quartz veinlets and trains of lenticular veinlets

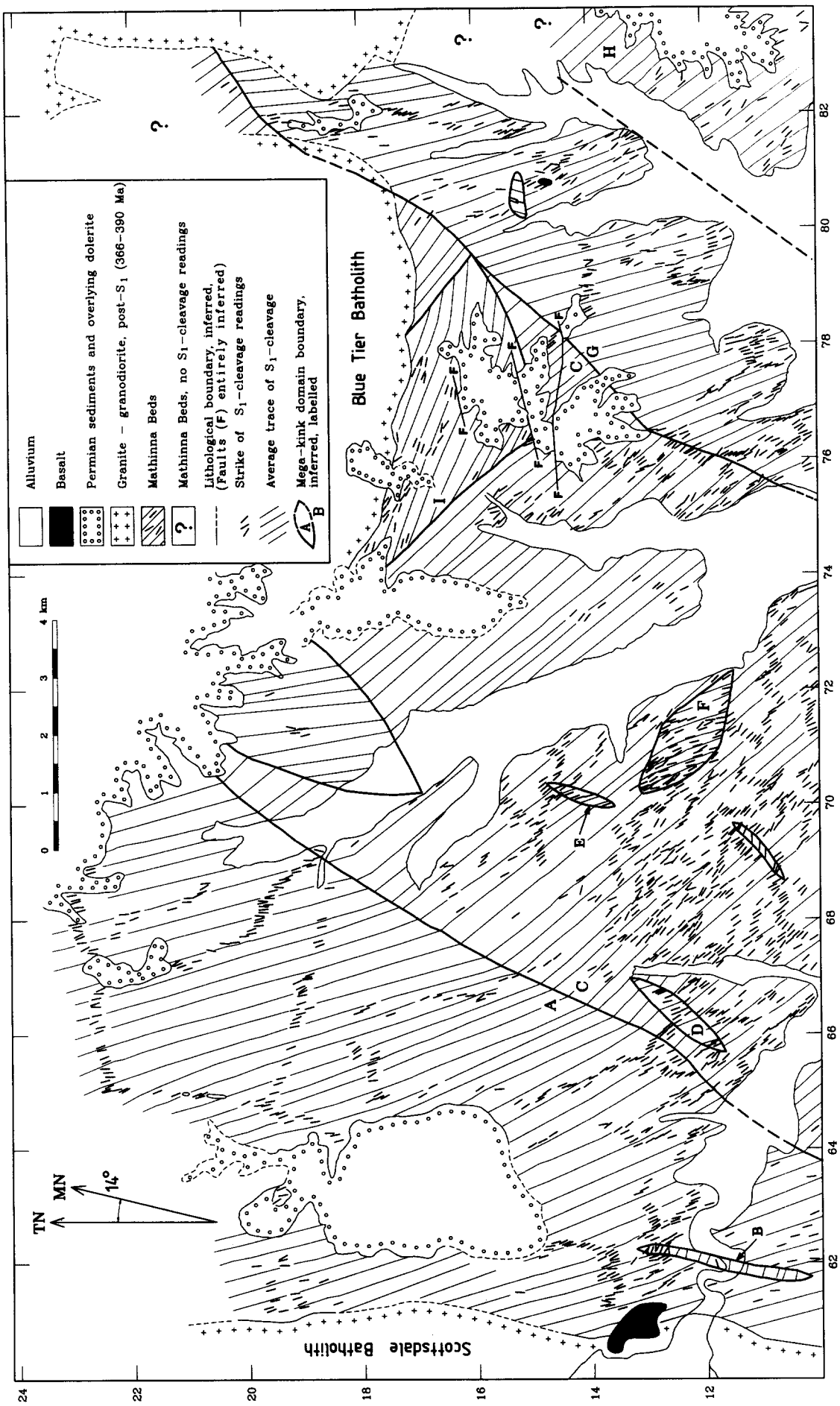

Fig. 5. Structural trend map of S_1-cleavage in the Mathinna Group from the area mapped in detail. All faults (F) are interpretive.

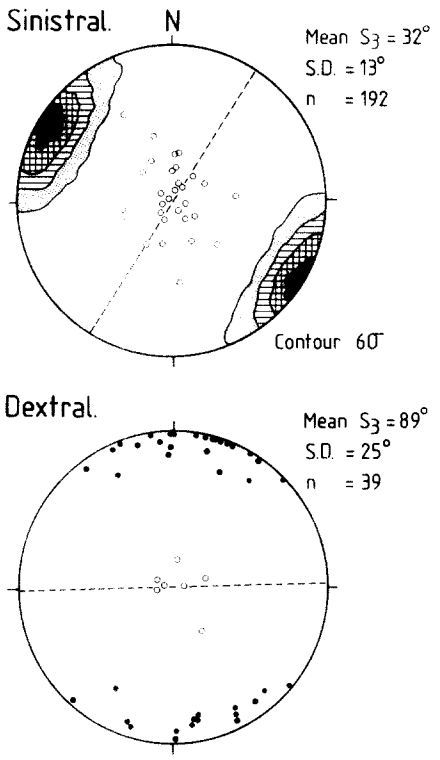

Fig. 6. Lower-hemisphere equal-area stereoplots of small-scale kink-band orientations from the area mapped in detail. Solid dots and contours are poles to kink-band axial surfaces (S_3); mean strike is given as a dashed line. Open circles are kink-band axes.

occur throughout the internal volume of the kink-band. These are oriented near-perpendicular to the kink axial surface. The axis of dilation associated with these veinlets is consistent with their formation in the earliest stages of kinking, with later rotation to their present orientation by the subsequent development of the kink-band.

D_3 *principal shortening direction derived from small-scale kink-bands*

The orientation of kink-bands, either single or as conjugate sets, is directly related to the relative orientation (ϕ, Fig. 3) of the principal shortening direction (Z) of the strain ellipsoid and the external S_1 cleavage surface (Gay & Weiss 1974). Only in the case of pure shear is Z coincident with the principal compressive stress (σ_1); such cases are rare in natural systems (Paterson 1989, Stubley 1990). Two methods have been used to estimate the palaeo-D_3 principal shortening direction based on average small-scale kink-band geometries in different domains.

(1) Kinking experiments performed by Gay & Weiss (1974) on a card deck and slate, define the relationship between both ϕ and α, and ϕ and ψ. Average α and ψ values of small-scale sinistral kink-bands for each domain from the area mapped in detail have been compared with the experimental data of Gay & Weiss (1974) (Fig. 10). These yield two estimates of ϕ and consequently two solutions for the Z-direction with respect to the external S_1 (Appendix 1). Z-directions based on α-data are consistently clockwise of and within 5–27° of those based on ψ-data from the same domain (Fig. 11 and Appendix 1). The principal shortening axis can be assumed to be horizontal because of the steep nature of kink-bands throughout the major part of NE Tasmania.

(2) The orthogonal bisector between conjugate sinistral and dextral kink-bands approximates (±20°, Stubley 1990) the Z-axis (Ramsay 1962). The trend of the Z-axis was estimated for most domains based on the bisector of the average strike of sinistral and dextral kink-band populations in each domain (Fig. 11 and Appendix 1). This method assumes coeval generation of sinistral and dextral kink-bands. This has not been confidently established, though it is thought to be the case because Z-axes by this method are consistent with results based on the data of Gay & Weiss (1974). Furthermore, conjugate kink-bands reported from domain C (Threader 1967) formed by 140°-trending shortening, which is coincident with estimates in this same domain by this study (Appendix 1).

The results of all three methods for each domain and group of domains have been listed in Appendix 1 and presented in Fig. 11. These data illustrate a systematic spread of the axes from SSE–NNW to ESE–WNW for results derived progressively from SSE–NNW to SE–NW and to E–W domains (Fig. 11). This is consistent with the small-scale kink-bands having been rotated by the megakinks, indicating progressive deformation up in scale with time.

To define the regional shortening direction during small-scale kinking the effect of late-stage megakinking needs to be removed by unfolding to the regional pre-megakinking S_1-strike (157°; the strike in SSE–NNW domains). The effect of megakinking on Z-axes have been removed in domains B (unfolded 44°) and C (unfolded 17°) (Appendix 1 and Fig. 11). These unfolded Z-directions are identical to those in the SSE–NNW domains (those not rotated by megakinking). The average Z-direction for all SSE–NNW domains and unfolded B and C domains are; 178°, 161° and 158° for the methods based on α-data, ψ-data and conjugate sets, respectively. Consequently, the principal shortening axis during small-scale kinking trends 166° ± 10° in a horizontal plane. This is close to the N–S-shortening that gave rise to megakinks (Powell *et al.* 1985) and small-scale kink-bands (Stubley 1990) in the Lachlan Fold Belt.

The spread in Z-direction for any given method and from different domains is small (6–21°) compared to the potential errors inherent in the methods used (i.e. the large spread in Gay & Weiss (1974) experimental data and assumptions pertaining to the pure shear model of Ramsay (1962). Thus the internal consistency of our orientation suggests that this result is reliable.

It should be noted that estimates of the Z-direction derived from conjugate kink-bands (Ramsay 1962) give orientations consistently anticlockwise of estimates calculated by the method of Gay & Weiss (1974) based on α-data (Fig. 11). This suggests that the geometry of

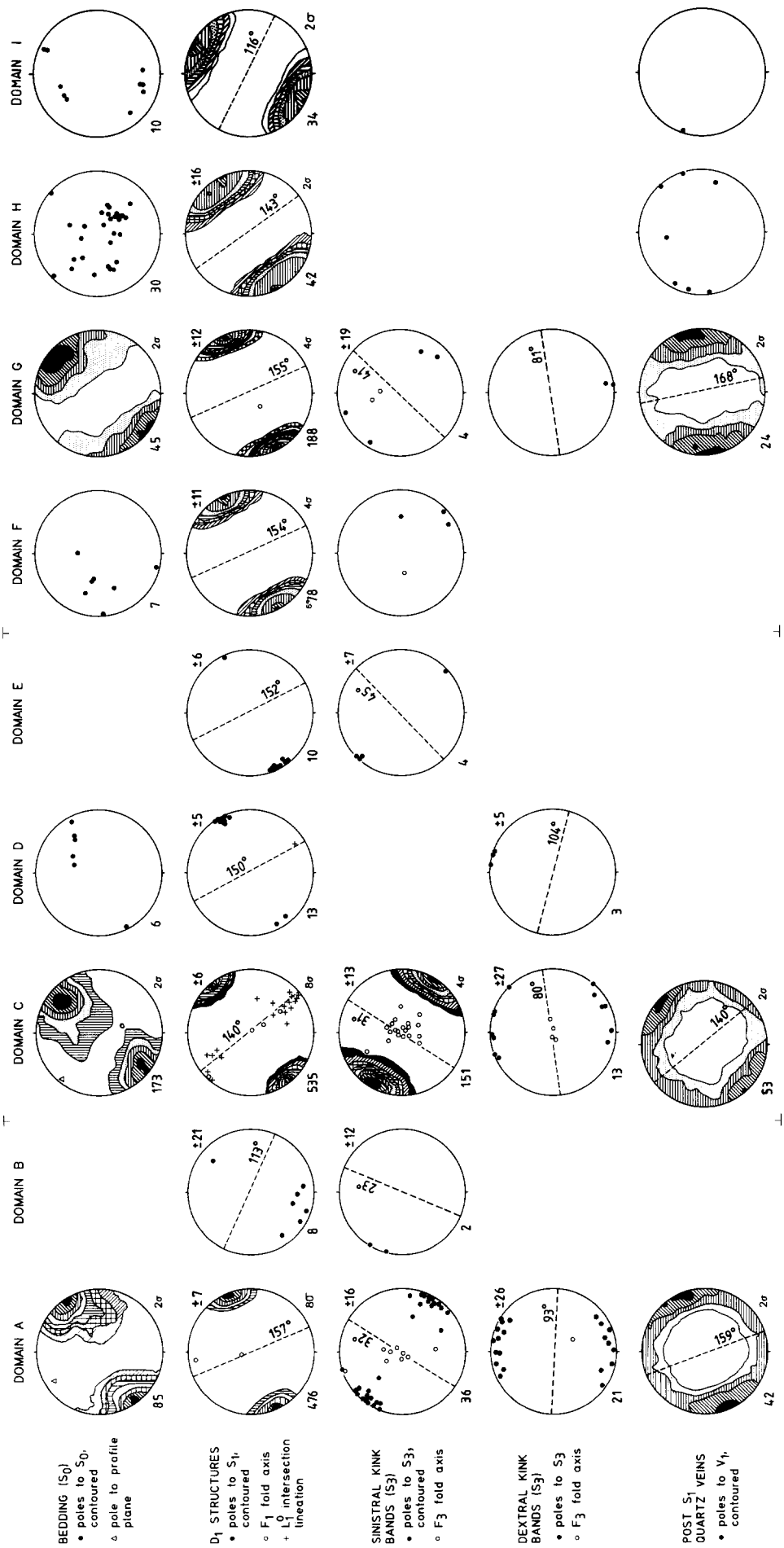

Fig. 7. Lower-hemisphere equal-area projections of structural data in each domain (Fig. 5) from the area mapped in detail. All planes plotted as poles. Contouring by the program STEREONET v4.0 (Allmendinger 1989). Number of readings in lower left-hand corner and contour interval in lower right-hand corner. Mean strikes are given as dashed lines and standard deviation is given in the top right-hand corner.

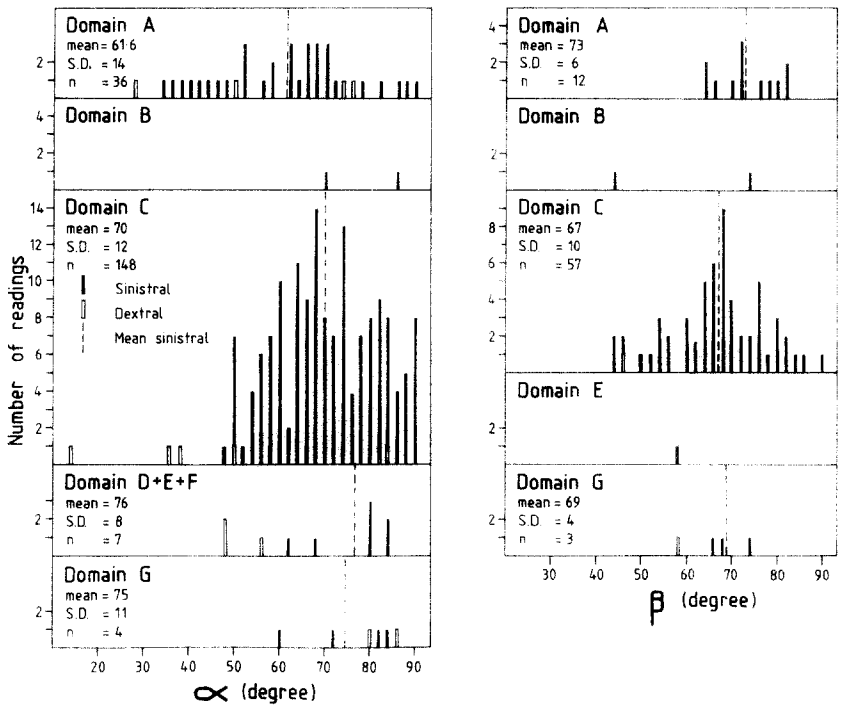

Fig. 8. Distribution of α and β angle (Fig. 3) measurements in each domain and groups of domains from the area mapped in detail. Means and standard deviations are given for sinistral data only.

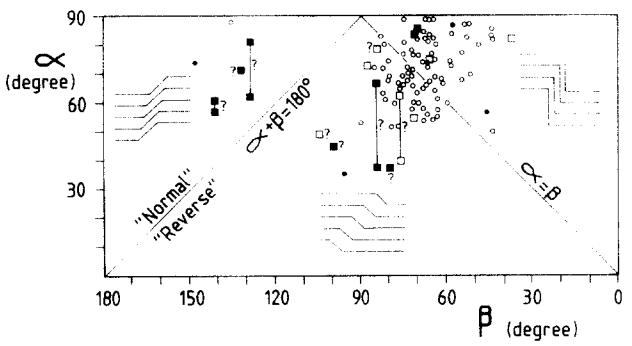

Fig. 9. Plot of α vs β from small-scale kink-bands from the area mapped in detail (circles). Megakink (α, β) data given by squares, unreliable megakink data indicated by (?) (see Appendix 2). Solid symbols are dextral data, open symbols are sinistral data((plot modified after Suppe (1985)).

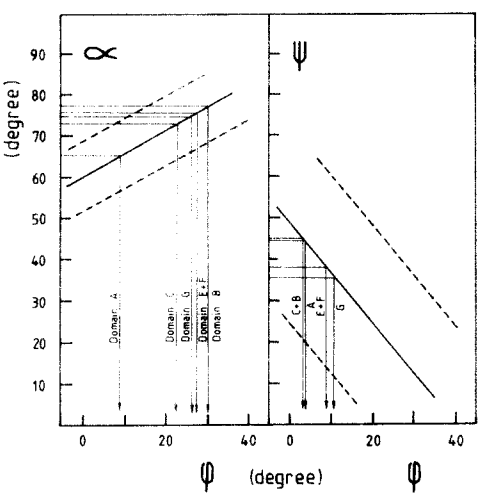

Fig. 10. Plot of the best-fit lines (solid) relating ϕ to α and ψ angles after the experimental data of Gay & Weiss (1974). Dashed lines are 95% confidence limits. Arrowed lines outline estimates of ϕ for specific domains and groups of domains from average α and ψ data (Appendix 1).

individual kinks in the area studied may display a consistent deviation from the pure shear kinking model of Ramsay (1962). This variation is also indicated by both ϕ and α being greater than for the ideal (constant volume) case. This is illustrated by the kinks plotting off the $\alpha = \beta$ line in the volume-loss field (Fig. 9). This may indicate that the small-scale kinks formed in a non-coaxial environment and not by pure shear (Stubley 1990).

Bulk shear strain and shear environment during small-scale kinking

The shear strain within an individual kink-band can be calculated if the rotation of the internal foliation with respect to the external foliation (ψ) is assumed to be due to simple shear (Fig. 3). In such a model the kink axial surfaces are equivalent to the shear plane and shear strain is given by the relationship:

$$\gamma = \tan \psi \text{ (Ramsay \& Graham 1970).} \quad (1)$$

Shear strain across the small-scale kink-bands have been calculated and plotted in Fig. 12. The average of the total group is approximately 0.92, which is consistent with constant volume kink-band formation ($\gamma \leq 1$). A significant proportion of small-scale kink-bands have shear strains exceeding 1 (Fig. 12). This is due to either late-stage rotation of the kink-band as a whole with respect to the external foliation (Kimura *et al.* 1989) and/or a result of tightening of the kink-band past the optimum constant volume ($\alpha = \beta$) geometry (Fig. 9) by further rotation of the internal foliation.

Rotation of the kink-band as a whole, with respect to

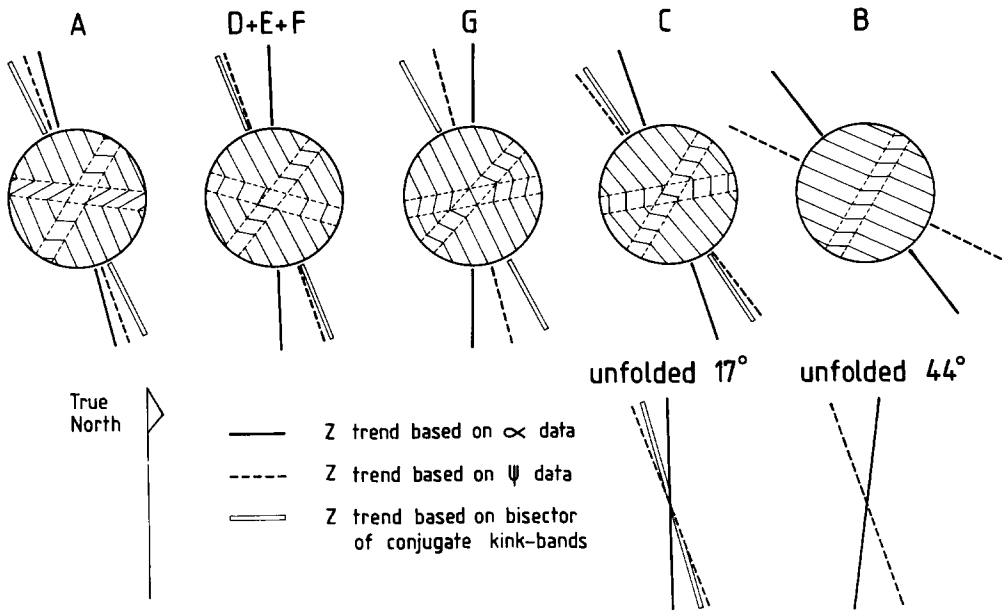

Fig. 11. Summary of the average relationship between average sinistral and dextral small-scale kink-bands in each domain (Fig. 5) and the calculated principal shortening axes (Z) indicated. Principal shortening axes in domains B and C have been rotated below to restore the Z-axes to before megakinking.

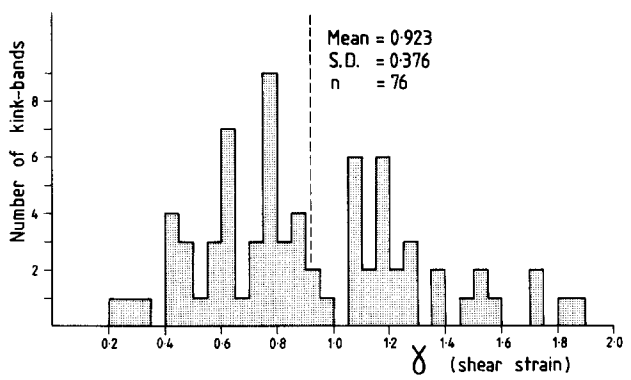

Fig. 12. Histogram of shear-strain data from individual small-scale kink-bands, calculated by the method of Ramsay & Graham (1970) by the analogy of the kink-band being a zone of simple shear.

the external foliation, to give rise to increasing ψ values (and thus shear strain) would involve a decrease in α whilst β remained constant. The Tasmanian kink-bands however show a general scatter of decreasing β and increasing α values (Fig. 9) and so do not support late-stage rotation of the kink-band with respect to the external foliation. However, the $\alpha > \beta$ kink-band geometry is consistent with tightening of the kink-band during kinking. Progressive tightening would result in rotation of the internal foliation to ψ values >45° with a minimal change in orientation of the kink-band with respect to the external foliation. Thus the shear-strain values for small-scale kink-bands (Fig. 12) are suggestive of progressive deformation with further strain being partitioned into pre-existing kink-bands; possibly during megakinking.

It is argued that the progressive tightening of the small-scale kink-bands is due to their formation by non-coaxial progressive deformation and not by pure shear. The predominance of sinistral kink-bands over dextral kink-bands and paucity of conjugate sets is due to the Z-direction being slightly oblique and consistently clockwise of the external S_1 foliation (Gay & Weiss 1974, Stubley 1990). This is born out by the average Z-direction being 9° clockwise from the regional S_1 strike. This obliquity and dominance of sinistral kink-bands is not consistent with pure shear experiments and so suggests a non-coaxial flow environment by comparison to the experimental work of Williams & Price (1990). The $\alpha > \beta$ morphology of the small-scale kink-bands indicates that they experienced progressive rotation of the internal S_1 foliation after initial kink-band formation. Such a geometry differs from natural and experimental kink-bands formed in pure shear environments (Paterson & Weiss 1962, 1966, Anderson 1964). This difference is possibly due to kinking occurring in a non-coaxial environment (Kimura *et al.* 1989, Stubley 1990) and not by pure shear.

It is proposed that the progressive non-coaxial flow that was experienced by small-scale kink-bands occurred during the latter-stage megakinking. The internal volume of the megakink (i.e. the rotated domain) can be considered as a zone experiencing non-coaxial flow during megakinking. Thus during megakinking additional strain was partitioned into pre-existing small-scale kink-bands as rotation by megakinking created domains of non-coaxial flow.

MAP-SCALE MEGAKINKING

General features

A very high density of S_1 readings in the Mathinna Group was obtained from the region mapped in detail in the central portion of NE Tasmania. These data were sufficient to accurately outline a series of kilometric- and

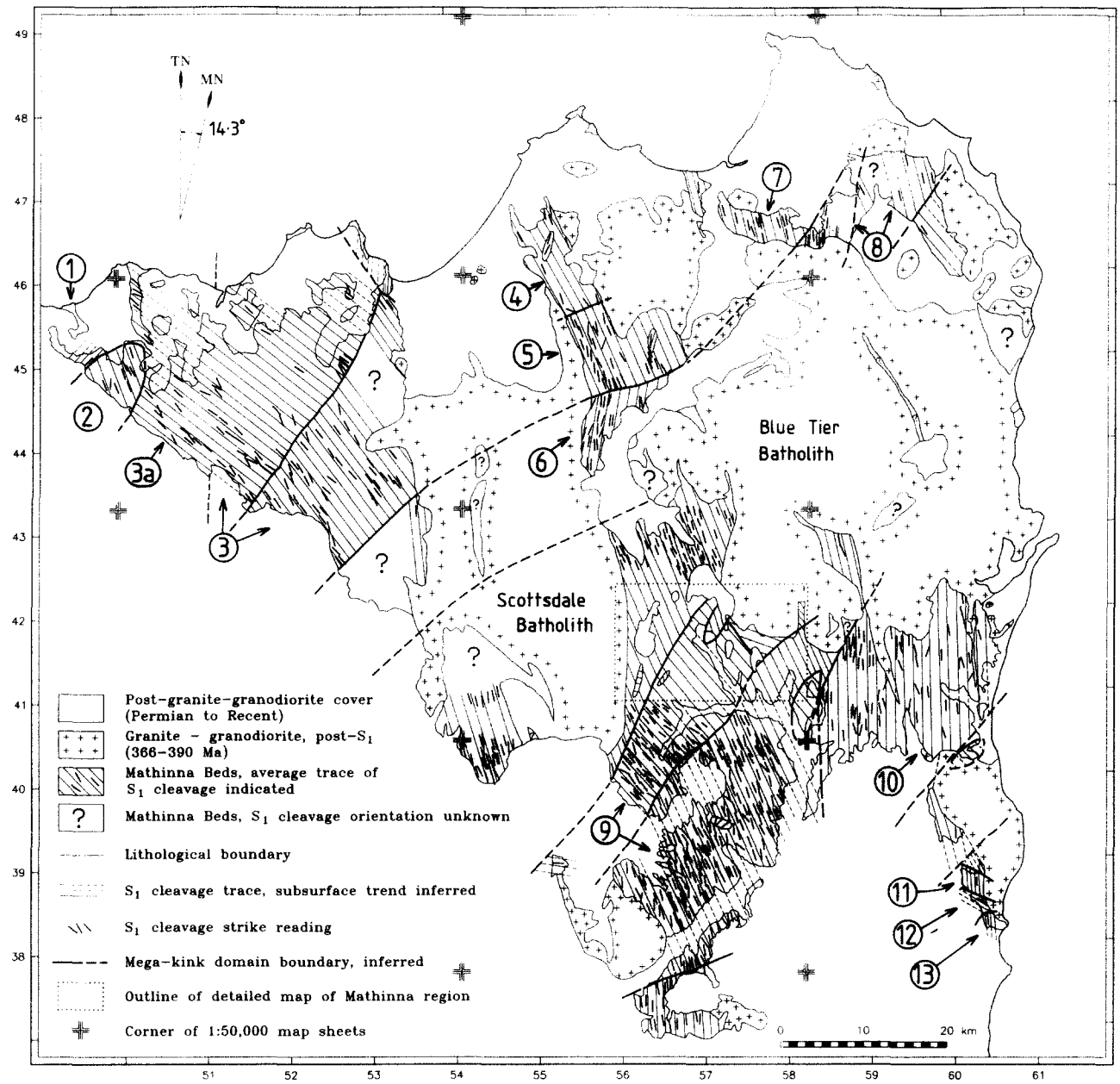

Fig. 13. Structural trend map of S_1-cleavage in the Mathinna Group from throughout NE Tasmania. Data compiled from the following 1:50,000 and 1:63,000 geological map sheets published by the Tasmanian Department of Mines: Noland Bay, Boobyalla, Eddystone, Blue Tier, Ringarooma, Pipers River, Launceston, Ben Lomond, St Helens, St Marys, Alberton and Snow Hill. Structural domains referred to in Fig. 14 are indicated.

decametric-scale kink-bands (Fig. 5). Kink-band boundaries are defined by relatively sharp changes in S_1 orientation and the kink-bands have an angular monoclinic geometry. The structural domains bounded by the fold axial surfaces of these megakinks have tightly constrained S_1 orientations, typically with standard deviations of 1–13° (Fig. 7). These structural domains have been divided into groups on the basis of their average S_1 strike (Fig. 5 and Appendix 1).

Similar scale megakinks have been documented by Turner in McClenaghan *et al.* (1982) and Turner & Calver (1987) from the southeast part of NE Tasmania and immediately north of the study area. All published S_1 cleavage orientation data from the Mathinna Group of NE Tasmania have been summarized in Figs. 13 and 14. These data show large regions of relatively constant S_1 orientation (±12–20° variation in each domain) bound by sharp planar zones across which the S_1 orientation has rotated (ψ) between 11° and 42° averaging 28° (Appendix 2). Consequently, the boundaries between these domains define the axial trace of megakinks. Like small-scale kink-bands, the axial surface of the megakinks are thought to also dip subvertically because of their straight traces across significant topographic relief. Megakink axial surfaces can be followed as far as 35 km along strike. Isolated megakink surfaces can be extrapolated through granitoid batholiths to connect with other axial traces of the same rotation sense and trend, making up a single axial surface trace as long as 100 km (Fig. 13).

There is no evident map-scale effect of D_3 megakinking on the Upper Devonian granitoid batholiths. The majority of D_3 strain is envisaged to have been par-

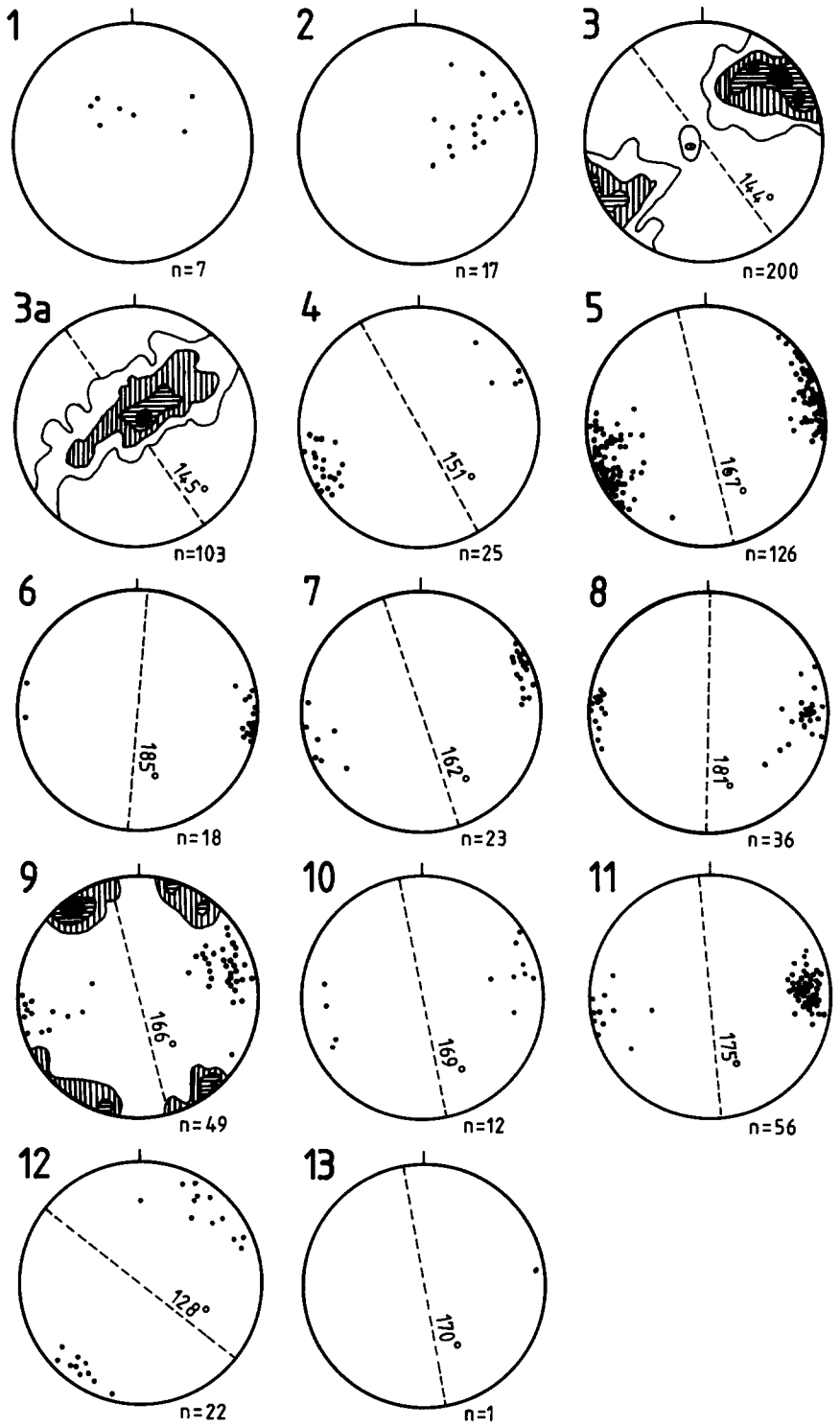

Fig. 14. Lower-hemisphere equal-area projections of poles to S_1 (dots and contoured) from NE Tasmania and poles to axial surfaces of small-scale kink-bands in domain 9 only (48 readings, contoured). Location of domains (labelled upper left-hand corner) indicated in Fig. 13. Contour intervals are 1, 3, 7 and 10%, 1% area, no 1% contour in domain 9. Dashed lines are average strike of S_1 cleavage. Data from Longman & Everard (1966), Marshall *et al.* (1969), Gee *et al.* (1979), Lennox (1980), McClenaghan *et al.* (1982), Baillie *et al.* (1986) and Turner & Calver (1987).

titioned into the Mathinna Group, being the less competent and having the pre-existing anisostropy of S_1. Any component of D_3 strain that was partitioned into the batholiths would not have involved ductile deformation of the batholiths as a whole because of their large size and subsequent shapes. The envisaged mode of any potential D_3 deformation of the granitoids is of a more localized nature, such as the development of faults and shear zones. Gee & Groves (1974) report a conjugate sets of thin (1–40 mm) mylonitic shear zones in the Piccanniny Point Adamellite. It is not known if these shears formed during D_3 kinking.

Conversely, the granitoid bodies themselves undoubtedly had an influence on the geometry of the megakinks. This is suggested by the broad range of megakink geometries (Appendix 2) when compared to the tightly con-

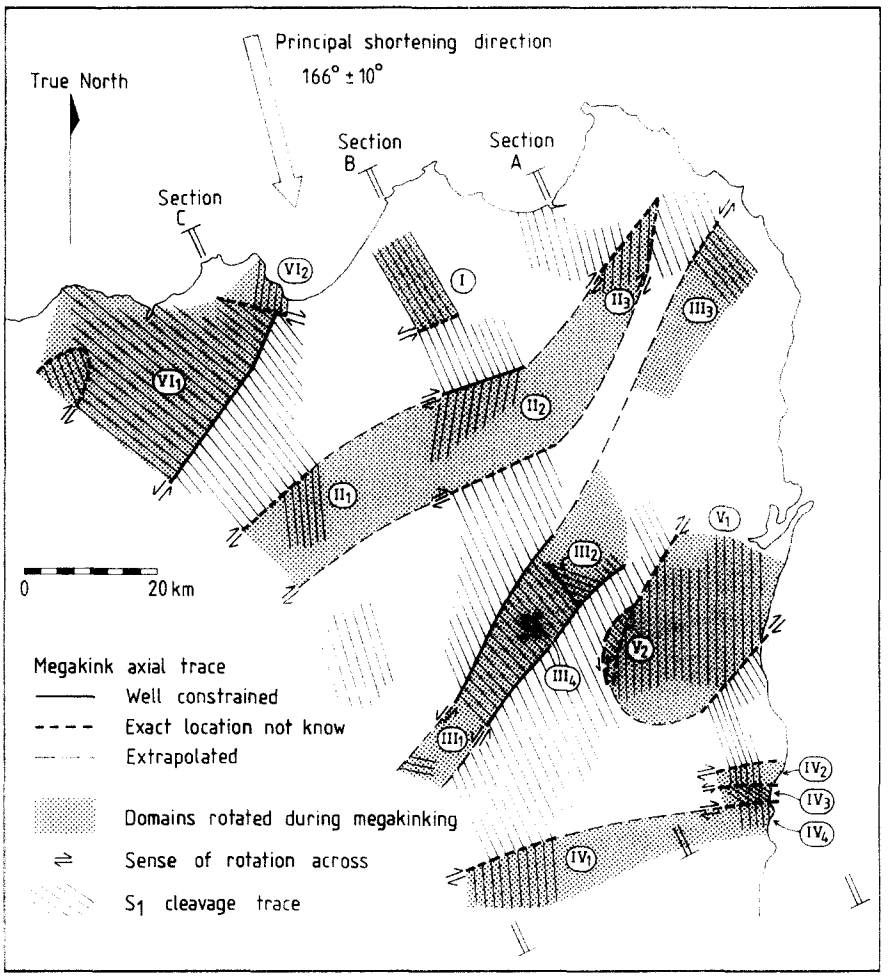

Fig. 15. Simplified map of megakink boundaries in NE Tasmania with the regions rotated from the regional NNW–SSW trend outlined (stippled) and labelled. The approximate geometric parameters of rotated regions are summarized in Appendix 2. The principal shortening direction is derived from small-scale kink-bands (Fig. 11 and Appendix 2). Section lines trend 157° parallel to the regional pre-kinking S_1 trace.

strained geometries of small-scale kink-bands (Fig. 9 and Appendix 1). Furthermore, the E–W domain I (Fig. 5) is most plausibly due to a relatively high degree of N–S shortening at the southern margin of the Blue Tier Batholith.

We can determine which of the domain groupings constitute the rotated domains (i.e. megakink-band) and which constitute the non-rotated domains (the pre-kink S_1 trend) by analysis of S_1 trends across NE Tasmania. The SSE–NNW domains are held to represent the pre-kinking structural trend in NE Tasmania since:

(1) the average strike of outcrop-scale sinistral kink-bands (032°) (Fig. 6) is identical to the overall trend of domain III_1 and III_3 (Fig. 15) which also displays sinistral rotation with respect to the adjacent structural domains. Consequently, these domains are considered as a sinistral megakink-band;

(2) the N–S domains; II_2, IV_1, IV_2 and IV_4 (Fig. 15), have experienced dextral rotation and the domains themselves trend ENE–WSW like the small-scale dextral kink-bands. Thus these domains are interpreted as dextral megakink-bands and the adjacent SSE–NNW domains have not rotated appreciably.

The domains that experienced bulk rotation relative to adjacent SSE–NNW domains during megakinking are shaded and labelled in Fig. 15 and interpreted as megakink-bands. The S_1 strike of each of the non-rotated domains lie between 144° and 167° and the average is 157° (Appendix 2) which is thus the average pre-kinking trend of S_1 for the whole of NE Tasmania.

Principal shortening direction

The approximate geometrical parameters, as smoothed out on a regional-scale, of the megakink-bands labelled in Fig. 15 are collated in Appendix 2. The range of α, β and ψ values of all these megakinks is larger than the range of the small-scale kink-bands. This reflects both the gross simplification of reducing these large structures to average parameters and the inaccuracy in constraining the trend of the axial trace of many of the kink folds (Fig. 15 and Appendix 2). The amount of rotation of S_1 during megakinking (average $\psi = 28°$; Appendix 2) is very low compared with the rotation of S_1 by the small-scale kinking (average $\psi = 42°$; Appendix 1). This indicates lesser bulk-shear strains and shortening across individual megakinks compared with that in the small-scale kink-bands (Appendix 1 and 2). α angles for megakink-bands are in the same range as for small-scale kink-bands. However, the combination of low ψ

angles and slightly higher α angles in some megakinks, results in some megakink β angles exceeding 90° (Fig. 9). Consequently, some megakink-bands have 'normal' geometry in contrast to the 'reverse' kink-band geometry displayed by small-scale kink-bands (Fig. 9).

'Normal' megakink-bands are restricted to the most easterly and western sections of megakink-band II and to V. The orientation of the axial surface of these 'normal' megakink-bands (and thus the α and β angles) are not well constrained (Fig. 15, compare to Fig. 13). Thus the geometric parameters presented for megakink-band domains II_1, II_3 and V_1 are possibly meaningless in terms of distinguishing these as having 'normal' or 'reverse' geometries. The best constrained axial surfaces of megakink-bands are in the central section through NE Tasmania (Fig. 15 and Appendix 2); these have 'reverse' geometries and orientations similar to the small-scale kinks. Consequently, the megakinks are interpreted to have formed in the same strain field as the small-scale kink-bands, with a 166°-trending principal shortening axis.

Relative timing of small-scale and mega-scale kinks

The relative timing of megakinking with respect to small-scale kink-bands can only be postulated on geometric arguments. Powell *et al.* (1985) argue that the constant angular relationships of small-scale kink-bands relative to the external S_1 (i.e. α angles) in all domains is consistent with their formation before and not during megakink rotation. Average strike of both sinistral and dextral small-scale kink-bands in domains B and C are consistent with their rotation due to megakinking after their original formation in orientations equivalent to those in the non-rotated SSE–NNW domains.

An early phase of formation of small-scale kink-bands and their subsequent rotation by megakinking is also supported by the principal shortening axis derived from small-scale kink-bands in different structural domains (Fig. 11). For example, calculated Z-axes in domains B and C, when megakink effects have been removed, are unfolded to orientations coincident to the Z-axis in non-rotated domains (Fig. 11). Furthermore, small-scale kink-bands have geometries consistent with progressive shortening after initial formation, this is compatible with late-stage megakinking. Progressive kinking up in scale, such as this, was also postulated by Powell *et al.* (1985) for the Lachlan Fold Belt.

D_3 BULK SHORTENING

We derive the following relationship (Goscombe & Findlay 1989) for the shortening across a kink-band, along an axis parallel to the external S_1 strike, assuming constant S_1 length:

$$\text{shortening ratio} = 1 - \cos\psi \text{ (Fig. 3).} \quad (2)$$

Shortening values across individual megakinks in NE Tasmania are listed in Appendix 2. These range from 3 to 29% and average 12.7%. The results in Appendix 2 have been used to calculate the crustal shortening due to megakinking along three sections parallel to the regional S_1 trend (157°), through NE Tasmania (Fig. 15). The proportion of the length of each of these three sections that involved megakink rotation ranges 40–47%. This data combined with the shortening ratios of individual megakinks gives rise to shortening values of 4.2, 3.3 and 2.2% for sections A, B and C, respectively.

Average shortening across individual small-scale sinistral kink-bands is of the order of 25% (Appendix 2). The average width of small-scale kink-bands is 23 mm. The average spatial density is 2.11 kink-bands m^{-1} along a section parallel to S_1. These values give rise to an average shortening across NE Tasmania by small-scale kink-bands of only 1.5%. This compares with the shortening by small-scale kink-bands in the Lachlan Fold Belt, estimated by Cudahy (1986) to average 2–5% at individual localities and to be between 1 and 3% regionally (Powell *et al.* 1985).

The sum of the shortening due to both small-scale and mega-scale kinking across NE Tasmania is in the order of 4–5%. This is considered a minimum estimate because shortening due to kinks of 1–10 m scale have not been considered. However, intermediate scales of kinking are rare and only developed in domains that were rotated during megakinking, thus possibly contributing <1% of shortening. Consequently, total D_3 shortening of NE Tasmania along a 157°-trending section is approximately 4–5%, which is equivalent to only 5–6 km of shortening across the region. This is compatible with the 5% total N–S-shortening in the Lachlan Fold Belt during kinking (Powell *et al.* 1985).

DISCUSSION AND CONCLUSIONS

Profuse small-scale kink-bands and mega-scale kink-bands occur throughout the Ordovician–Devonian Mathinna Group in NE Tasmania. Both scales of kinking occurred under 166°-trending bulk shortening and formed together in the same orogeny. Domains of small-scale kink-bands were rotated by megakinks, indicating progressive deformation up in scale. Progressive tightening of small-scale kink-bands was accommodated by further rotation of the internal S_1 foliation, after initial kink-band formation, in a non-coaxial flow environment. This additional tightening may be due to additional strain being partitioned into pre-existing small-scale kink-bands during late-stage rotation of domains by megakinking, these rotated domains themselves being zones of non-coaxial flow.

Kinking post-dates Middle Devonian granodiorite batholiths and pre-dates the Parmeener Supergroup; that is D_3 kinking occurred between 300 and 375 Ma (and possibly <356 Ma). The principal shortening direction during D_3 kinking trended 166° ± 10° in a horizontal plane. D_1 tight folding and D_2 over-thrusting both involved intense shortening along a ENE–WSW-trending horizontal axis. D_1 occurring prior to the St Marys

Porphyrite (i.e. before 388 Ma) and D_2 immediately after. Thus D_3 kinking occurred both as a temporally distinct event and in a strain field nearly orthogonal to that during D_1 and D_2. Consequently, kinking in NE Tasmania cannot be considered a late-stage episode of the same tectonic cycle as D_1–D_2 but as a new tectonic event.

Bulk shortening of 4–5% during D_3 kinking is very small particularly in comparison to the possible maximum shortening of 30–55% during D_1. Such a small component of crustal shortening could not result in thickening of the crustal profile. Features indicative of dilation parallel to the kink axes (such as veinlets orthogonal to kink axes and stretching lineations) have not been recognized, thus it is assumed there was no extension parallel to the kink axes. Because kink axes are subvertical, all of the SSE–NNW D_3 shortening must have been accommodated by ENE–WSW crustal extension with no vertical thickening.

All features of D_3 kinking are similar to those in the Lachlan Fold Belt, where centimetre- and kilometre-scale kinking occurred at approximately 330 Ma under N–S-directed shortening of only 5%. The recognition of this same tectonic event not only throughout the Lachlan Fold Belt but as far south as Tasmania, supports the suggestion of Powell *et al.* (1985) that D_3 kinking involved a continent-wide stress field. This further supports the hypothesis that NNW–SSE-shortening in eastern Australia may be related to the N–S-shortening in central Australia during the Carboniferous Alice Springs Orogeny (Powell *et al.* 1985).

The D_3 kinks in central NE Tasmania formed at crustal levels of 120 ± 45 MPa pressure (4.2 km depth). At these crustal levels, temperatures of only 79–173°C are experienced for a normal crustal geotherm of 30°C km^{-1}. Such shallow crustal levels are entirely consistent with the concept of kinks as brittle and 'instantaneous' structures. The small component of shortening (4–5%) responsible for D_3, suggests that kinks developed in NE Tasmania only as a consequence of the acute angle (9°) between the principal shortening axis and the trend of the pre-existing S_1 cleavage. Kinks would not have developed if bulk shortening was directed at a high angle to the S_1 cleavage, resulting instead in flattening across the S_1 cleavage. Consequently, steeply plunging mega-kinks may be typical of late-stage shallow crustal tectonics involving minimal shortening only if the principal shortening axis is aligned at very low angles to the pre-existing structural grain of the region.

Acknowledgements—Emyr Williams and Tom Blenkinsopp are thanked for very useful discussions and comments. The Deputy Director of the Tasmanian Department of Mines, Rod Hargraves, is thanked for making the facilities available for this study, particularly the drafting of some figures and arranging microprobe time at the University of Tasmania. C. W. Passchier, M. P. Stubley, C. McA. Powell and an anonymous reviewer are thanked for careful and pertinent comments that greatly enhanced this paper.

REFERENCES

Allmendinger, R. W. 1989. STEREONET v4.0; a plotting program for orientation data for the Macintosh™ Plus, SE and II computers. Cornell University, New York.

Anderson, T. B. 1964. Kink bands and related geological structures. *Nature* **202**, 272–274.

Baillie, P. W. *et al.* 1986. Geological survey explanatory report, Eddystone. Sheet 25(8516S), 1:50 000 series. Tasmanian Department of Mines.

Baillie, P. W. *et al.* 1989. The Eastern Tasmania Terrane. In: *Geology and Mineral Resources of Tasmania* (edited by Burrett, C. F. & Martin, E. L.). *Spec. Publ. geol. Soc. Aust.* **15**, 234–237.

Bucher-Nurminen, K. 1987. A recalibration of the chlorite–biotite–muscovite geobarometer. *Contr. Miner. Petrol.* **96**, 519–522.

Cocker, J. D. 1982. Rb–Sr geochronology and Sr isotopic composition of Devonian granitoids, eastern Tasmania. *J. geol. Soc. Aust.* **29**, 139–158.

Cudahy, T. J. 1986. Mesoscopic structures associated with the Bermagui Megakink. *Aust. J. Earth Sci.* **33**, 503–517.

Dewey, J. F. 1965. Nature and origin of kink-bands. *Tectonophysics* **1**, 459–494.

Gay, N. C. & Weiss, L. E. 1974. The relationship between principal stress directions and the geometry of kinks in foliated rocks. *Tectonophysics* **21**, 287–300.

Gee, R. D. & Groves, D. I. 1974. Contact structures at a granodiorite intrusion, Piccaninny Point northeast Tasmania. *R. Soc. Tasman. Pap. Proc.* **107**, 47–52.

Gee, R. D. & Legge, P. J. *et al.* 1979. Geological survey explanatory report, Beaconsfield. 1 mile series, sheet 30(8215N). Tasmanian Department of Mines.

Goscombe, B. D. & Findlay, R. H. 1989. Mega-kinking in the Mathinna Beds, Northeast Tasmania. *Tasman. Dept Mines Rep.* **1989/42**.

Goscombe, B. D., McClenaghan, M. & Everard, J. 1992. Contact metamorphism of the Mathinna Beds and the depth of crustal residence during mega-kinking in Northeast Tasmania. *Tasman. Dept Mines Rep.* **1992/34**.

Hoisch, T. D. 1989. A muscovite–biotite geothermometer. *Am. Miner.* **74**, 565–572.

Hollister, L. S., Grissom, G. C., Peters, E. K., Stowell, H. H. & Grisson, V. B. 1987. Confirmation of the empirical correlation of Al in hornblende with pressure of solidification of calc-alkaline plutons. *Am. Miner.* **72**, 231–239.

Johnson, M. C. & Rutherford, M. J. 1989. Experimental calibration of the aluminium-in-hornblende geobarometer with application to Long valley caldera (California) volcanic rocks. *Geology* **17**, 837–841.

Kimura, G., Koga, K. & Fujioka, K. 1989. Deformed soft sediments at the junction between the Mariana and Yap Trenches. *J. Struct. Geol.* **11**, 463–472.

Laird, J. 1989. Chlorites: metamorphic petrology. In: *Micas. Rev. Miner. Min. Soc. Am.* **19**, 405–453.

Lennox, P. 1980. Ben Lomond sheet Mathinna Beds. Unpublished draft report. Tasmanian Department of Mines.

Longman, M. J. & Everard, G. 1966. Geological survey explanatory report, Launceston. 1 mile series. Tasmanian Department of Mines.

Marshall, B. *et al.* 1969. Geological survey explanatory report, Pipers River. 1 mile series, sheet 30 (8315N). Tasmanian Department of Mines.

Massone, H. J. 1989. The upper thermal stability of chlorite + quartz: an experimental study in the system MgO-Al2O3-SiO2-H2O. *J. metamorph. Geol.* **7**, 567–581.

Massonne, H. J. & Schreyer, W. 1987. Phengite geobarometry based on the limiting assemblage with K-feldspar, phlogopite and quartz. *Contr. Miner. Petrol.* **96**, 212–224.

McClenaghan, M. P. *et al.* 1982. Geology of the Ringarooma–Boobyalla area. *Tasman. Dept Mines. Geol. Surv. Bull.* **61**.

Paterson, M. S. & Weiss, L. E. 1962. Experimental folding in rocks. *Nature* **195**, 1046–1048.

Paterson, M. S. & Weiss, L. E. 1966. Experimental deformation and folding in phyllite. *Bull. geol. Soc. Am.* **77**, 343–347.

Paterson, S. R. 1989. A reinterpretation of conjugate folds in the central Sierra Nevada, California. *Bull. geol. Soc. Am.* **100**, 248–259.

Powell, C. McA. & Baillie, P. W. 1992. Tectonic affinity of the Mathinna Group in the Lachlan Fold Belt. *Tectonophysics* **214**, 193–209.

Powell, C. McA., Cole, J. P. & Cudahy, T. J. 1985. Megakinking in the Lachlan Fold Belt, Australia. *J. Struct. Geol.* **7**, 281–300.

Powell, M. & Powell, R. 1977. Plagioclase-alkali-feldspar geothermometry revisited. *Mineralog. Mag.* **41**, 253–256.

Powell, R. & Holland, T. J. B. 1988. An internally consistent dataset

with uncertainties and correlations: 3. Applications to geobarometry, worked examples and a computer program. *J. metamorph. Geol.* **6**, 173–204.
Powell, R. & Holland, T. J. B. 1990. Calculated mineral equilibria in the pelite system, KFMASH (K_2O–FeO–MgO–Al_2O_3–SiO_2–H_2O). *Am. Miner.* **75**, 367–380.
Ramsay, J. G. 1962. The geometry of conjugate fold systems. *Geol. Mag.* **99**, 516–526.
Ramsay, J. G. & Graham, R. H. 1970. Strain variation in shear belts. *Can. J. Earth Sci.* **7**, 786–798.
Rixon, L. K., Bucknell, W. R. & Rickard, M. J. 1983. Megakink folds and related structures in the Upper Devonian Merrimbula Group, South Coast, N.S.W. *J. geol. Soc. Aust.* **30**, 277–293.
Spear, F. S. & Cheney, J. T. 1989. A petrogenetic grid for pelitic schists in the system SiO_2–Al_2O_3–FeO–MgO–K_2O–H_2O. *Contr. Miner. Petrol.* **101**, 149–164.
Stewart, K. G. & Alvarez, W. 1991. Mobile-hinge kinking in layered rocks and models. *J. Struct. Geol.* **13**, 243–259.
Stubley, M. P. 1990. The geometry and kinematics of a suite of conjugate kink bands, southeastern Australia. *J. Struct. Geol.* **12**, 1019–1031.
Suppe, J. 1985. *Principles of Structural Geology*. Prentice-Hall, New Jersey, 336–340.
Threader, V. M. 1967. The geology of the Mangana–Waterhouse goldfields with particular reference to structure and mineralization. Unpublished M.Sc. thesis, University of Tasmania.
Turner, N. J., Black, L. P. & Higgins, N. C. 1986. The St Marys Porphyrite and related dykes—a Devonian intra-caldera ignimbrite and its feeder. *Aust. J. Earth Sci.* **33**, 201–218.
Turner, N. J. & Calver, C. R. 1987. Geological survey explanatory report, St Marys. 1:50 000 series, sheet 49(8514N). Tasmanian Dept. of Mines.
Weiss, L. E. 1980. Nucleation and growth of kink bands. *Tectonophysics* **65**, 1–38.
Williams, P. F. & Price, G. P. 1990. Origin of kink bands and shear-band cleavage in shear zones: an experimental study. *J. Struct. Geol.* **12**, 145–164.

APPENDIX 1

Table A1. Average geometries of small-scale kink-bands and estimates of the trend of the principal shortening axis for individual domains and groups of domains from the area mapped in detail (Fig. 5). Average shear strains and shortening estimates are also included. All orientations are with respect to true north. The sample sets for β readings are often less than the totals at the top of the table. Standard deviations in Fig. 7

Domain	A	B	C	D	E	F	G	D + E + F	Means
Domain grouping	SSE–NNW	E–W	SE–NW	◄---------- SSE–NNW ----------►					
n = sinistral (sin.)	36	2	151	—	4	3	4	7	
n = dextral (dext.)	21	—	13	3	—	—	2	3	
sin./(sin. + dext.)	0.63	1.00	0.92	0.00	1.00	1.00	0.67	0.70	
Average external S_1 strike	157°	113°	140°	150°	152°	154°	155°	—	
Average S_3 strike sinistral	033°	031°	031°	—	045°	036°	041°	038°	032°*
Average S_3 strike dextral	095°	—	083°	104°	—	—	081°	104°	089°*
Average α sinistral	065°	078°	073°	—	077°	075°	075°	076°	
Average α dextral	060°	—	058°	050°	—	—	083°	050°	
Average β sinistral	073°	059°	067°	—	058°	—	069°	058°	
Average β dextral	150°	—	071°	—	—	—	058°	—	
Average ψ sinistral	44.5°	45.0°	45.0°	—	38.0°	—	35.7°	38.0°	0.41°
Average ψ dextral	44.0°	—	44.3°	—	—	—	37.0°	—	0.42°
Z-direction after Gay & Weiss (1974), based on average sinistral kink-band α data.									
ϕ (Fig. 10)	9°	30°	22°	—	30°	26°	26°	27°	
Strike of Z-axis	166°	143°	162°	—	182°	180°	181°	179°	
Unfolded strike of Z	166°	187°	179°	—	182°	180°	181°	179°	178°
Z-direction after Gay & Weiss (1974), based on average sinistral kink-band ψ data.									
ϕ (Fig. 10)	3.9°	2.9°	2.9°	—	8.3°	—	10.7°	8.3°	
Strike of Z-axis	161°	116°	143°	—	160°	—	166°	160°	
Unfolded strike of Z	161°	160°	160°	—	160°	—	166°	160°	161°
Z-direction after Ramsay (1962), bisector of conjugate set of average kink-band strikes.									
Strike of Z-axis	154°	—	147°	—	—	—	152°	161°	
Unfolded strike of Z	154°	—	164°	—	—	—	152°	161°	158°
Shear strain (γ) for average kink-bands after method of Ramsay & Graham (1970). γ = tan ψ.									
Mean γ sinistral	1.039	1.016	0.904	—	0.781	—	0.726	0.781	0.921
Mean γ dextral	0.966	—	2.740	—	—	—	0.754	—	0.957
Shortening parallel to external S_1 across average sinistral kink-band = (1 − cos ψ).									
Shortening (using ψ above)	28.7%	29.3%	29.3%	—	21.2%	—	18.8%	21.2%	
Mean ψ (= 180 − (α + β))†	42°	43°	40°	—	45°	—	36°	46°	
Shortening (use mean ψ)	25.7%	26.9%	23.4%	—	29.3%	—	19.1%	30.5%	
Shortening (average of both)	27.2%	28.1%	26.3%	—	25.2%	—	18.9%	25.9%	25.3%

*Average of total dataset, see Fig. 6.
†Mean ψ is calculated from the average α and β values, not the average of ψ readings.

APPENDIX 2

Table A2. Collation of the approximate geometries of megakinks in NE Tasmania. Average S_1 strikes are from stereonet data where available (Figs. 7 and 14), otherwise from Fig. 13. Megakink domains (those rotated during kinking) are labelled as in Fig. 15. These parameters must be considered with caution because they are based on over simplification of kinking in NE Tasmania into simple geometric domains. Furthermore, the orientation of the megakink axial trace is poorly constrained for many megakinks (Figs. 13 and 15). All orientations with respect to true north and in degrees, shortening as percent. Domains VI_1 and VI_2 are in the shallowly inclined region near Pipers River

Kink domain (Fig. 15)	I	II_1		II_2		II_3		III_1	III_2	III_3	III_4	IV_1	IV_2		IV_3		IV_4	V_1		V_2		VI_1	VI_2	Means
Shear sense	sin	dext		dext		dext		sin	sin	sin	dext	dext	dext		sin		dext	dext		sin		sin	dext	
Kink-band geometry*	rev†	norm†		rev		norm†		rev	rev	rev†	rev	rev	rev†		rev†		rev†	norm†		rev†		rev	rev†	
S_1 strike in rotated domain	151	175		185		184		140	116	140	154	180	175		128		170	180		143		129	180	
Megakink axial trace (S_3)	66†	46†		75		43†		32	50	35†	98	70	90†		90†		90†	48†		40†		37	100†	
Margin (north/south)	S	N	S	N	S	N	S	Average	S	N	Average	N	N	S	N	S	N	N	S	N	S	Average	Average	
S_1 strike outside megakink	167	144	164	167	157	162	166	157	155	166	140‡	157	157	128‡	175‡	170‡	128‡	155	158	155	180‡	144	145	157 (not ‡)
Calculated α	79	82	62	88	82	61	57	55	75	49	42	87	67	38	85	80	38	73	70	65	40	73	45	65.5
Calculated β	85	129	129	70	70	141	141	72	66	105	56	70	85	85	38	38	80	132	132	77	77	88	100	
Calculated ψ	16	−31	−11	18	28	−22	−18	17	39	24	14	23	18	47	47	42	42	−25	−22	12	37	15	35	28 (not norm)
Shortening parallel to the external $S_1 = 1 - \cos\psi$																								
Based on each margins ψ	3.9	14.3	1.8	4.9	11.7	7.3	4.9	4.4	22.3	8.6	3.0	7.9	4.9	31.8	31.8	25.7	25.7	9.4	7.3	2.2	20.1	3.4	18.1	
Average for megakink	3.9	←8.1→		←8.3→		←6.1→		4.4	22.3	8.6	3.0	7.9	←18.4→		←28.8→		25.7	←8.4→		←17.9→		3.4	18.1	12.7

*Kink-band geometry after (Dewey 1965): 'reverse' is $\alpha + \beta < 180°$, 'normal' is $\alpha + \beta > 180°$.
†Estimate of orientation of the kink axial trace is essentially unconstrained (see Fig. 13), thus kink-band geometry is also unconstrained.
‡S_1 strike not equivalent to regional pre-kinking strike because these domains are kink-bands within kink-bands.